

# Comparing dynamical and photometric-stellar masses of early-type galaxies at $z \sim 1$ <sup>★</sup>

A. Rettura<sup>1,2,3</sup> <sup>★★</sup>, P. Rosati<sup>1</sup>, V. Strazzullo<sup>1,6</sup>, M. Dickinson<sup>4</sup>, R.A.E. Fosbury<sup>5</sup>, B. Rocca-Volmerange<sup>2,3</sup>, A. Cimatti<sup>7</sup>, S. di Serego Alighieri<sup>7</sup>, H. Kuntschner<sup>5</sup>, B. Lanzoni<sup>8</sup>, M. Nonino<sup>9</sup>, P. Popesso<sup>1,5</sup>, D. Stern<sup>10</sup>, P.R. Eisenhardt<sup>10</sup>, C. Lidman<sup>11</sup>, and S.A. Stanford<sup>12,13</sup>

<sup>1</sup> European Southern Observatory, Karl Schwarzschild Strasse 2, Garching bei Muenchen, D-85748, Germany

<sup>2</sup> Université Paris-Sud 11, Rue Georges Clemenceau 15, Orsay, F-91405, France

<sup>3</sup> Institut d'Astrophysique de Paris, UMR7095 CNRS, Université Pierre & Marie Curie, 98bis Bd Arago, 75014 Paris, France

<sup>4</sup> NOAO, 950 North Cherry Avenue, P.O. Box 26732, Tucson, AZ 85726-6732, United States

<sup>5</sup> ST-ECF, Karl-Schwarzschild-Strasse 2, D-85748 Garching, Germany

<sup>6</sup> Dipartimento di Scienze Fisiche, Università degli Studi di Napoli "Federico II", via Cinthia, I-80126 Napoli, Italy

<sup>7</sup> Istituto Nazionale di Astrofisica (INAF), Osservatorio Astrofisico di Arcetri, Largo E. Fermi 5, 50125 Firenze, Italy

<sup>8</sup> Istituto Nazionale di Astrofisica (INAF), Osservatorio Astronomico di Bologna, via Ranzani 1, 40127 Bologna, Italy

<sup>9</sup> Istituto Nazionale di Astrofisica (INAF), Osservatorio Astronomico di Trieste, via G. B. Tiepolo 11, I-34131 Trieste, Italy

<sup>10</sup> Jet Propulsion Laboratory, California Institute of Technology, 4800 Oak Grove Drive, Pasadena, CA 91109; United States

<sup>11</sup> European Southern Observatory, Alonso de Cordova 3107, Vitacura, Casilla 19001, Santiago 19, Chile

<sup>12</sup> Department of Physics, University of California at Davis, 1 Shields Avenue, Davis, CA 95616-8677; United States

<sup>13</sup> Institute of Geophysics and Planetary Physics, Lawrence Livermore National Laboratory, L-413, P.O. Box 808, 7000 East Avenue, Livermore, CA 94551; United States

Preprint online version: July 15, 2018

## ABSTRACT

**Aims.** The purpose of this study is to explore the relationship between galaxy stellar masses, based on multiwavelength photometry spectral template fitting and dynamical masses based on published velocity dispersion measurements, for a sample of 48 early-type galaxies at  $z \sim 1$  with *HST*/ACS morphological information.

**Methods.** We determine photometric-stellar masses and perform a quantitative morphological analysis of cluster and field galaxies at redshift  $0.6 < z < 1.2$ , using ground- and space-based multiwavelength data available on the GOODS-S field and on the field around the X-ray luminous cluster RDCS1252.9-2927 at  $z = 1.24$ . We use multi-band photometry over  $0.4\text{--}8\mu\text{m}$  from *HST*/ACS, *VLT*/ISAAC and *Spitzer*/IRAC to estimate photometric-stellar masses using Composite Stellar Population (CSP) templates computed with PEGASE.2 (Fioc & Rocca-Volmerange, 1997) models. We compare stellar masses with those obtained using CSPs built with Bruzual & Charlot (2003; BC03) and Maraston (2005; M05) models. We then compare photometric-stellar mass and dynamical mass estimates as a function of morphological parameters obtained from *HST*/ACS imaging.

**Results.** Based on our sample, which spans the mass range  $\log M_{\text{phot}} \approx [10, 11.5]$ , we find that 1) PEGASE.2, BC03, M05 yield consistent photometric-stellar masses for early-type galaxies at  $z \sim 1$  with a small scatter (0.15 dex rms); 2) adopting a Kroupa IMF, photometric-stellar masses match dynamical mass estimates for early-type galaxies with an average offset of 0.27 dex; 3) assuming a constant IMF, increasing dark matter fraction with the increasing galaxy mass can explain the observed trend; 4) we observe that early-type galaxies with significant disk components (Sa/Sab) or with signs of dynamical interaction tend to have the largest deviation from a one-to-one  $M_{\text{dyn}} \text{ vs } M_{\text{phot}}$  relation.

**Key words.** galaxies: clusters: individual: RDCS J1252-2927 - galaxies: evolution - galaxies: formation - galaxies: elliptical and lenticular, cD - galaxies: kinematics and dynamics - cosmology: observations.

Send offprint requests to: A. Rettura, arettura@eso.org

<sup>★</sup> Observations have been carried out using the Very Large Telescope at the ESO Paranal Observatory under Program IDs: LP168.A-0485, 169.A-0458, 170.A-0788, 70.A-0548

<sup>★★</sup> Present address: Department of Physics and Astronomy, Johns Hopkins University, 3400 N. Charles Str., Baltimore, MD 21218, USA

## 1. Introduction

Galaxy surveys have traditionally built samples based on the luminosities of galaxies, and have used luminosity functions to study the evolution of the galaxy population. The need to select galaxies on the basis of their (stellar or possibly

total) mass and to trace the evolution of the space density of galaxies in mass bins has long been advocated. In such a way, one can reconstruct the build-up of galaxy mass across cosmic time and directly compare observations to predictions of currently favored hierarchical structure formation models. The evolution of the galaxy luminosity function is generally affected in a complex fashion by all the physical processes which modulate the star formation history of galaxies, whereas the mass function evolves in a smoother way and is a direct probe of galaxy formation models (e.g., Baugh et al. (2003), Hernquist & Springel (2003), Somerville et al. (2004), Nagamine et al. (2004), De Lucia et al. (2005)). This has motivated many authors during the last decade to carry out surveys by selecting galaxies at near-infrared rest-frame wavelengths (e.g., Songaila et al. (1994), Cohen et al. (1999), Drory et al. (2001), Cimatti et al. (2002)), since the rest-frame near-IR light is closely related to the total mass (e.g., Gavazzi et al. (1996)).

More recently, the efficiency with which multi-wavelength photometry can be collected from ground-based and space-based observatories has enabled the measurement of stellar masses by fitting widely-sampled spectral energy distributions (SED) of galaxies with spectrum synthesis models (e.g., Brinchmann & Ellis (2000), Cole et al. (2001), Papovich et al. (2001), Shapley et al. (2001), Dickinson et al. (2003), Fontana et al. (2003), Rudnick et al. (2003), Fontana et al. (2004), Drory et al. (2004a), Saracco et al. (2004), Rocca-Volmerange et al. (2004)). In parallel, considerable efforts have been devoted to measuring the evolution of the mass-to-light ratio of galaxies out to  $z \sim 1$ , via Fundamental Plane studies (FP, Djorgovski & Davis (1987), Dressler (1987)) at different environmental densities (e.g. Franx (1993), van Dokkum & Franx (1996), Busarello et al. (1997), van Dokkum et al. (1998), Treu et al. (2001), Gebhardt et al. (2003), Treu et al. (2005), van der Wel et al. (2005), di Serego Alighieri et al. (2005)). These studies have provided increasing evidence that galaxy mass plays a critical role in driving galaxy evolution. While it has become common to derive stellar masses from multi-wavelength surveys via SED fitting methods (the so called photometric-stellar masses), it remains important to test the reliability of this methodology which relies heavily on stellar population spectrum synthesis models.

Moreover, by comparing dynamical and photometric-stellar masses one can investigate the relevance of the dark matter component of early-type galaxies as a function of the total mass (e.g., Napolitano et al. (2005)).

Drory et al. (2004b) have performed such a comparison for a large sample of local galaxies in the SDSS (York et al. 2000) spanning a large mass range,  $8 < \log(M_{phot}/M_{\odot}) < 12$ . In this paper, we extend their study to higher redshifts, inevitably focusing on massive systems with  $M_{phot} \geq 10^{10} M_{\odot}$ . For these galaxies, Drory et al. (2004b) find a good match between the photometric-stellar mass,  $M_{phot}$ , and a quantity  $M_{dyn} \propto \frac{\sigma_0^2 R_e}{G}$ , although with a substantial scatter around the line of equality. In a similar study, Lintott et al. (2005) have compared dynamical and photometric-stellar masses within the effective

radii of a sample of local massive ( $M_{phot} > 8 \cdot 10^{10} M_{\odot}$ ) early-type galaxies also selected from the SDSS. They find  $M_{dyn} \propto M_{phot}^{1.3}$ , suggesting that dark matter might become increasingly important in massive galaxies.

Cappellari et al. (2005) have studied the correlation between the dynamical  $M/L$  from virial and Schwarzschild modeling and the photometric-stellar mass (all of them within the effective radius) for a sample of early-type galaxies at  $z \sim 0$ , with high  $S/N$  integral field spectroscopy. They use Vazdekis et al. (1996), Vazdekis (1999) stellar synthesis models and assume a Kroupa (2001) IMF to compute photometric-stellar masses. They find the adoption of a Salpeter IMF to provide unphysical results, as a number of galaxies would have  $M_{phot} > M_{dyn}$  and note that  $\sim 30\%$  dark matter within the effective radius and/or IMF variations are needed to explain the discrepancies between the two mass estimators. This is consistent with earlier findings at  $z \sim 0$  from dynamical studies (e.g., Gerhard et al. (2001), Thomas et al. (2005)) and at  $z \sim 1$  from gravitational lensing (e.g., Treu & Koopmans (2004), Rusin & Kochanek (2005)).

Using total masses derived from gravitational lensing study of a sample of  $0.3 < z < 1.0$  early-type galaxies, Ferreras et al. (2005) note a transition from little or no dark matter in the inner regions (within the effective radius) to dark matter dominating in the outer regions in the massive early-type galaxies, whereas no such a trend is observed in lower mass galaxies.

On a sample of 17 early-type galaxies at  $z \sim 1$  di Serego Alighieri et al. (2005) find a good agreement between the two mass estimators for the high mass galaxies, but most of their lower mass galaxies have stellar masses larger than the dynamical ones.

Here, we significantly extend their work *i)* by using a sample almost a factor of 3 bigger, *ii)* by measuring in a homogeneous fashion structural parameters for the entire galaxy sample using deep *HST*/ACS data, and *iii)* by including rest-frame near-infrared photometry to estimate photometric-stellar masses. With the availability of *Spitzer*/IRAC (InfraRed Array Camera) data (Fazio et al. 2004), one can access the critical restframe near IR-domain at  $z \simeq 1 - 2$ , thus enabling a more accurate determination of photometric-stellar masses at redshifts where a significant fraction of the stellar mass is being assembled (e.g., Dickinson et al. (2003)).

This paper is organized as follows. In Sect. 2 we describe the sample selection; in Sect. 3 we present the dataset and describe the data analysis; in Sect. 4 we describe the morphological analysis based on *HST*/ACS images; in Sect. 5 we account for our method of deriving photometric-stellar masses for different spectrum synthesis models and discuss the results of their comparison; in Sect. 6 we derive dynamical masses and discuss their comparison with photometric-stellar estimates in sect. 7. And finally in Sect. 8 we summarize the results.

We assume a  $\Omega_{\Lambda} = 0.73$ ,  $\Omega_m = 0.27$  and  $H_0 = 71 \text{ km} \cdot \text{s}^{-1} \cdot \text{Mpc}^{-1}$  flat universe (Spergel et al. 2003), and use magnitudes in the AB system throughout this work.

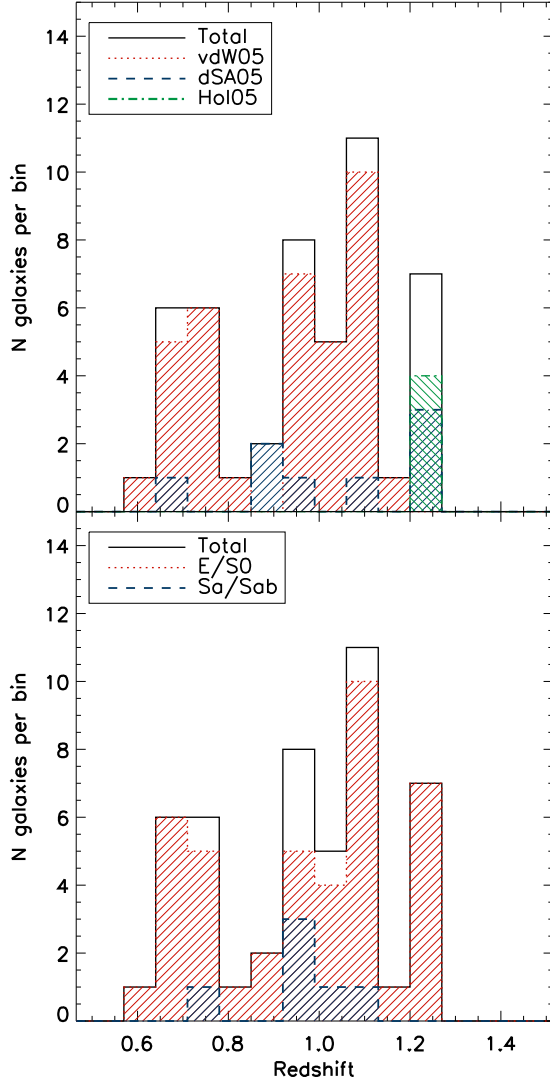


**Fig. 1.** Top panel: The galaxy redshift distribution of the whole sample, consisting of 48 galaxies (black line), is compared with the distribution of each sub-sample over-plotted in red, blue and green for vdW05, dSA05 and Hol05, respectively. Bottom panel: galaxy redshift distribution divided by morphological classes, 42 early-types (E/S0) (red) and 6 bulge-dominated spirals (Sa/Sab) (blue). Images of these 6 early-type spiral galaxies are shown in Fig. 2.

## 2. Sample selection

This work is based on imaging data from two fields which have extensive multiwavelength coverage over  $0.4 - 8\mu\text{m}$  from a combination of high-quality deep imaging with *HST*/ACS (Advanced Camera for Surveys), *VLT*/ISAAC, and *Spitzer*/IRAC: the Great Observatories Origin Deep Survey, GOODS-South field (Giavalisco et al. 2004) and the field around the cluster RDCS1252.9-2927 at  $z = 1.24$  (hereafter C11252; Rosati et al. 2004). In addition, accurate velocity dispersions of mostly early-type galaxies at  $z \sim 1$  have been published from studies of the Fundamental Plane in these two fields (van der Wel et al. 2005, Holden et al. 2005,

di Serego Alighieri et al. 2005), using deep *VLT*/FORS2 spectroscopy. Therefore, this data set provides a sample of distant galaxies spanning an adequate mass range, with high-quality morphological information, which is very well suited for a comparison of stellar-photometric masses with dynamical estimates.

Specifically, we selected

- 27<sup>1</sup> and 9 galaxies in the CDFS and CL1252 fields respectively from the work of van der Wel et al. (2005, hereafter vdW05),
- 8 CDFS galaxies from di Serego Alighieri et al. (2005, hereafter dSA05),
- 4 cluster member galaxies of C11252 from Holden et al. (2005, hereafter Hol05).

These targets were either color- (vdW05, Hol05) or spectroscopically- (dSA05) selected as early-type galaxies spanning a redshift range  $0.62 < z < 1.24$  (see Figure 1). As is customary in FP studies, velocity dispersions were measured in a normalized circular aperture with a diameter of  $2R_J = 1.19h^{-1}\text{kpc}$ , equivalent to  $3.4''$  at the distance of the Coma cluster, as described by Jorgensen et al. (1995).

Hence, our final sample consists of 48 galaxies with  $< z \gtrsim 1$ , with accurate velocity dispersions derived from *VLT*/FORS2 spectroscopy. The reader is referred to the aforementioned papers for object selection and coordinates and for a detailed description of the  $\sigma_0$  measurements. Galaxies in this sample have  $H$  absolute rest-frame magnitudes in the range  $-21.6 < M_H < -24.67$ , and rest-frame  $U - V$  colors  $1.35 < U - V < 1.99$ .

## 3. Cataloging and Data Analysis

In order to accurately study both the morphology and the SED of our galaxy sample at  $z \sim 1$ , a deep and homogeneous multi-wavelength dataset is needed.

The availability for both fields of deep *HST*/ACS imaging gives access to high quality galaxy morphologies and makes this dataset ideal for performing a reliable quantitative analysis. In order to obtain the morphological parameters in the rest-frame B-band (often used as a reference framework for morphological studies), we have used deep *HST*/ACS images taken with the *F850LP* filter for both fields. We expect the morphological  $k$ -correction, from restframe V- (for the lower redshift galaxies of our sample) to B-band, on the derived scale parameters to be small, in particular for early-type galaxies (e.g., Bohlin et al. (1991), Giavalisco et al. (1996), Kuchinski et al. (2000), Papovich et al. (2003)).

To build SEDs of galaxies of the GOODS-S field, we have used optical *HST*/ACS ( $B_{F435W}$ ,  $V_{F606W}$ ,  $i_{775W}$ ,  $z_{F850LP}$ ) (Giavalisco et al. 2004), *VLT*/ISAAC near infrared ( $J, K_s$ )

<sup>1</sup> The vdW05 and dSA05 samples have two sources in common in the CDFS with slightly different published measurements of  $\sigma_0$ . In this work, we adopt the values published in dSA05 as the spectroscopic data were also in hand.

(Vandame et al, in prep.) and *Spitzer*/IRAC ( $3.6\mu\text{m}$ ,  $4.5\mu\text{m}$ ,  $5.8\mu\text{m}$ ,  $8.0\mu\text{m}$ ) photometry (Dickinson et al., in prep.) which is publicly available through the GOODS collaboration<sup>2</sup>.

For field and cluster galaxies in the CL1252 field, we have used ground-based optical *VLT*/FORS2 ( $B$ ,  $V$ ,  $R$ ), space-based optical *HST*/ACS ( $i_{F775W}$ ,  $z_{F850lp}$ ) (Blakeslee et al. 2003), near infrared *VLT*/ISAAC ( $J_s$ ,  $K_s$ ) (Lidman et al. 2004) and *Spitzer*/IRAC ( $3.6\mu\text{m}$ ,  $4.5\mu\text{m}$ ) photometry (Stanford et al., in prep.).

Accurate PSF-matched photometry, i.e. photometric measurements normalized to the same aperture and angular resolution, is essential to build unbiased galaxy SEDs. To account for the large variations of the PSF throughout our dataset (from  $\approx 0.1''$  FWHM of *HST*/ACS to  $\sim 2''$  of *Spitzer*/IRAC), we first perform photometry in  $3''$  diameter apertures in each pass-band, we then apply aperture corrections out to  $7''$  radius. The latter are derived from a growth curve analysis of point-like sources (identified in the ACS images) in each passband. This approach is preferable to the one of smoothing all images to the worst angular resolution which can result in significant source blending. We note that the adopted aperture corrections out to a radius of  $7''$  allow more than 95% of the galaxy light to be recovered.

#### 4. *HST*/ACS morphologies of $z \sim 1$ early-type galaxies

A description of the surface brightness (SB) distribution of early-type galaxies is provided by the ‘Sérsic  $R^{1/n}$ ’ profile Sérsic (1968), with more luminous galaxies having larger Sérsic indices  $n$ , i.e., steeper light distribution towards the center (Caon et al. 1993, D’Onofrio et al. 1994, Graham et al. 1996). We have used GIM2D, a fitting algorithm for parameterized two-dimensional modelling of SB distribution (Simard 1998, Marleau & Simard 1998) to fit each galaxy light distribution of our entire sample with a Sérsic (1968) profile of the form:

$$I(r) = I_{e,n} \cdot 10^{-b_n[(r/R_{e,n})^{1/n} - 1]}, \quad (1)$$

where  $b_n = 1.99n - 0.33$  (Capaccioli 1989), and  $R_{e,n}$  is the effective radius (i.e., the projected radius enclosing half of the light). The classical de Vaucouleurs profile thus simply corresponds to  $n = 4$  and  $b_n = 7.67$  in eq.(1).

In this work, we allow  $n$  to span the range between 0 and 5, and the best-fitting parameters  $n$  and  $R_{e,n}$  are used both to describe the scale-lengths of the galaxies and to interpret their dynamical properties, as discussed in Section 6.

Derived values of  $n$  and  $R_{e,n}$  for galaxies in our sample are reported in Table 1. We note that even allowing the Sérsic index to range out to  $n=8$  the derived  $n$  are then found well below  $n=5.8$ .

We model each galaxy central PSF component with analytic functions derived from visually selected stars in the surrounding ( $30'' \times 30''$ ) region of each galaxy. A 2D radial multi-gaussian function has been fitted to tens of selected stars around

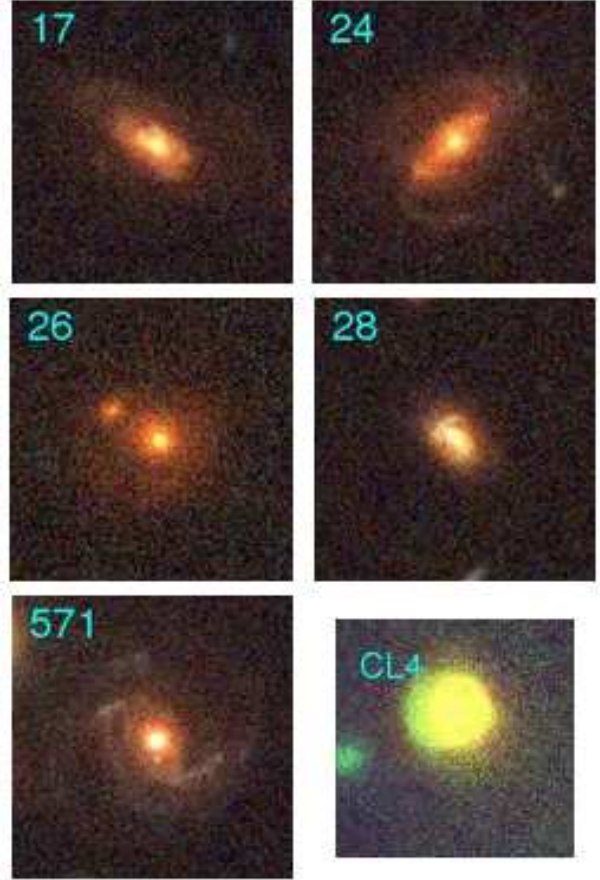


**Fig. 2.** Color ( $B, V, i, z$ ) images ( $5''$  across) of visually classified (Sa/Sab) early-type-spiral galaxies. The morphological analysis reveals the presence of an underlying stellar disk and/or a clear spiral-arm pattern for these sources. Shortened labels indicate objects CDFS-17, CDFS-24, CDFS-26, CDFS-28, CDFS-571 and CL1252-4 in our catalogue. Note that the set of color we use for CL4 is a different one ( $B, z, K_s$ ). We point out that the green crescent in CL4 is possibly a morphologically disturbed spiral arm.

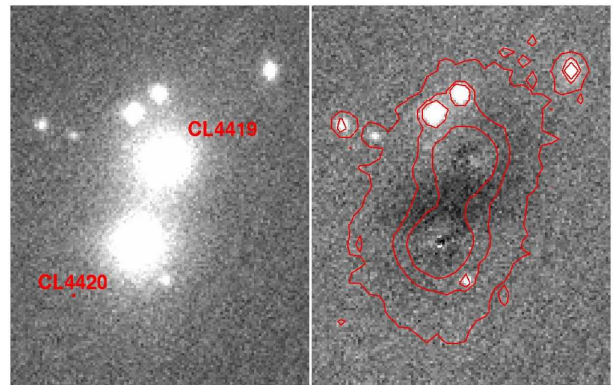


**Fig. 3.** Left: ACS  $z_{850lp}$  image of the central bright cluster galaxies (BCGs) of the X-ray luminous cluster CL1252 at  $z = 1.24$ . Right: Best-fit Sérsic-model-subtracted image of the same region of CL1252 which reveals signs of interaction in the form of an S-shaped residual linking the two galaxy centers.

<sup>2</sup> See <http://www.stsci.edu/science/goods/>



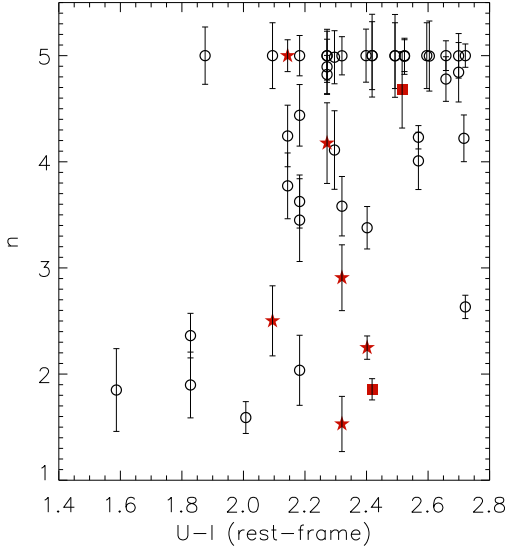


**Fig. 4.** The correlation of the Sérsic index,  $n$ , with the  $U-I$  rest-frame color (AB magnitudes). Filled red stars symbols indicate the bulgy-spirals subsample (see Fig. 2). Filled red squares indicate CL4419 and CL4420, the pair of BCGs of the cluster CL1252 at  $z = 1.24$  showing evidence of mutual dynamical interaction (see also Fig. 3).

each galaxy and outputs have been stacked together to provide an appropriate PSF image (for each galaxy) to be convolved to the galaxy best-fit 2D model to better reproduce each observed galaxy light profile. In this way, we also account for PSF variations over the ACS field. More details of our approach to modelling *HST*/ACS galaxy morphologies in the  $1.0 < z < 1.5$  range will be given elsewhere (Rettura et al., in preparation). The reliability and the accuracy of the morphological analysis from GOODS ACS data in the range of magnitudes and sizes probed by our sample is extensively discussed in Ravindranath et al. (2006).

In addition, as the sample we use was mainly spectroscopically and color selected, a visual analysis has also been performed to define a visual morphological classification. We identified 37 ellipticals (E), 5 lenticulars (S0) and 6 bulge-dominated spirals (Sa/Sab; see bottom panel of Fig. 1). Images of the 6 early-type-spiral galaxies are shown in Fig. 2. We also note that CL1252-4419 and CL1252-4420 are the central Bright Cluster Galaxies (BCGs) of CL1252 and are thought to be in mutual dynamical interaction (Blakeslee et al. 2003). As shown in Fig. 3, the subtraction of our Sérsic 2D-models for these two galaxies reveals evidence of such an interaction, in the form of an S-shaped residual that links the two galaxy centers. As shown in Fig. 4, we also find that  $n < 3$  systems tend to have bluer  $U-I$  rest-frame colors resulting in a bimodal distribution which is similar to what has been found shown by several authors (e.g. Kauffmann et al. (2003)).

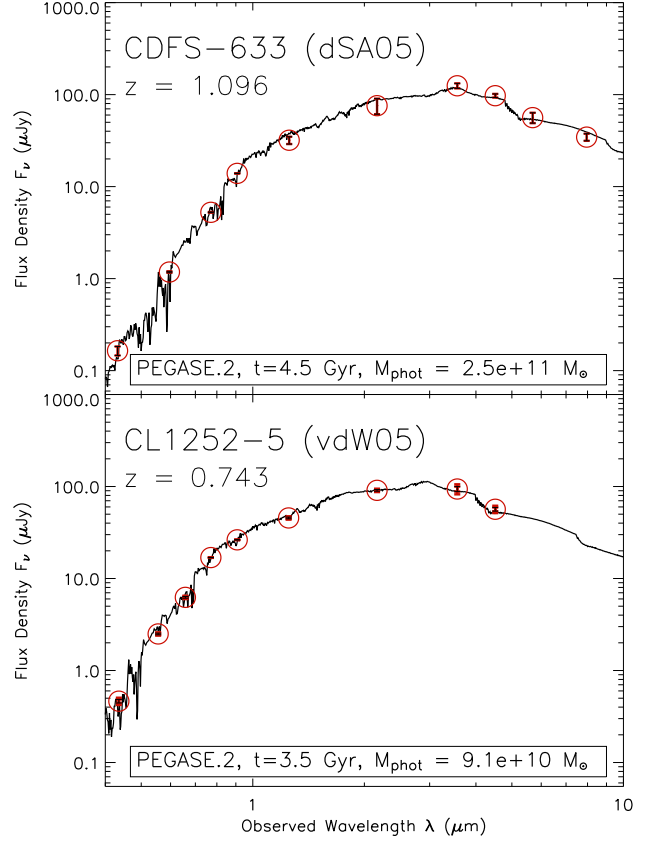


**Fig. 5.** SEDs of an early type galaxies at  $z \sim 1$  in each of our fields. The red open circles, with corresponding error bars, are observed flux densities in the *HST*/ACS ( $B_{F435W}$ ,  $V_{F606W}$ ,  $i_{775W}$ ,  $z_{F850LP}$ ), *VLT*/ISAAC ( $J_s, K_s$ ) and *Spitzer*/IRAC ( $3.6\mu m$ ,  $4.5\mu m$ ,  $5.8\mu m$ ,  $8.0\mu m$ ) passbands (top panel) and *VLT*/FORS2 ( $B$ ,  $V$ ,  $R$ ), *HST*/ACS ( $i_{775W}$ ,  $z_{F850LP}$ ), *VLT*/ISAAC ( $J_s, K_s$ ) and *Spitzer*/IRAC ( $3.6\mu m$ ,  $4.5\mu m$ ) passbands (bottom panel). As an illustration, best-fit PEGASE.2 models are also shown (black solid line). The best-fit mass and age estimates are reported in each panel. Average errors on ages are  $\pm 1$  Gyr, errors on masses are  $\sim 40\%$  (i.e., 0.15 dex).

## 5. Photometric-stellar masses at $z \sim 1$

### 5.1. Stellar mass determination

We derive stellar masses for each galaxy in our sample using multiwavelength matched aperture photometry from 10 and 9 passbands for the CDFS and CL1252 fields respectively. For each galaxy, we compare the observed SED with a set of composite stellar populations (hereafter, CSP) templates computed with PEGASE.2 models (Fioc & Rocca-Volmerange 1997). In Figure 5 we show the SEDs of two  $z \sim 1$  early type galaxies of our sample. As an illustration we over-plot the best-fit PEGASE.2 models from which the photometric-stellar mass is estimated.

The adopted grid of star formation history (SFH) scenarios has been shown to consistently reproduce observations of galaxy counts at  $z \sim 0$  from UV to optical wavelengths (Fioc & Rocca-Volmerange 1999), and to result in reliable photometric redshifts with the code Z-PEG

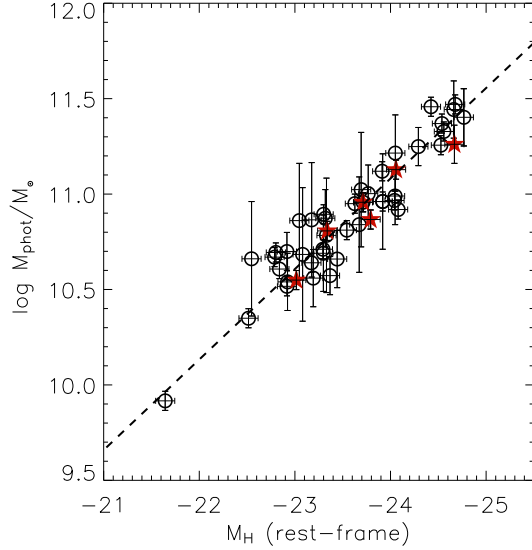


**Fig. 6.** Each galaxy best-fit model rest-frame  $H$ -band ( $\sim 1.6\mu\text{m}$ ) absolute magnitude,  $M_H$ , is plotted against derived photometric-stellar mass. The dashed line correspond to a straight-line fit to the data (see text). Filled red stars are used to indicate the bulge-dominated spirals sub-sample.

(Le Borgne & Rocca-Volmerange 2002). We assume a Kroupa (2001) IMF and dust-free model templates. In the template SEDs used here, the metallicity evolves consistently with the SFH: stars are gradually formed with the same metallicity as the ISM, reaching about solar values at the ages of interest in this study. We note that the stellar masses computed in this paper corresponds to the mass locked into stars plus the mass of the remnants (white dwarfs, neutron stars, black holes).

By comparing each observed SED with these atlases of synthetic spectra, we construct a 3D  $\chi^2$  space spanning a wide range of SFHs, ages and stellar masses. We adopted same template parameters as listed in Table 1 of Le Borgne & Rocca-Volmerange (2002). The age, SFH scenario and stellar mass of the model giving the lowest  $\chi^2$  are taken as the best-fit estimates of the galaxy luminosity-weighted age, SFH, and galaxy mass in stars. These photometric-stellar mass estimates take into account the evolution with galaxy age of the mass fractions for each template as described in Rocca-Volmerange et al. (2004) (see also their Fig. 3). The range of acceptable ages for a given galaxy has been limited by the age of the universe at its observed redshift. The errors on the ages and the masses are estimated by sampling the full probability distribution (i.e. a function of the 3-dimension space of free parameters). A 3D confidence region, around the measured best-fit values, is set to contain 68.3 % of the joint probability distribution of the free parameters. The errors correspond to the projections of the confidence region for 3 interesting parameters onto each free parameter axis. This procedure results in typical errors of galaxy ages about 1 Gyr and typical uncertainties on the mass determination of about  $\sim 40\%$  (i.e., 0.15 dex). The derived estimates of photometric-

stellar masses for each galaxy are summarized in Table 1.

It remains well known that the derived stellar masses depend on the adopted star formation history.

We have also investigated the effect of dust extinction on the best-fit photometric-stellar masses by including a fourth free parameter,  $0.0 < E(B - V) < 0.4$ , following the Cardelli et al. (1989) prescription. By performing the fit on 28 galaxies for which IRAC photometry is available in all 4 bands, we find that in  $\sim 40\%$  of the cases  $E(B - V) = 0$  gives the best fit. In the remaining cases, masses which are lower by  $0.2 \pm 0.1$  dex are found, with corresponding  $E(B - V) \leq 0.2$ . This test supports the validity of the dust-free model assumption, as also widely used in the literature for early-type galaxies.

Many authors have pointed out that the use of the near-IR luminosity may allow a more secure determination of stellar masses, as IRAC photometry samples the rest-frame near IR-domain in this particular redshift range. This corresponds to  $H$ -band rest-frame wavelengths where the galaxy luminosity is dominated by the old stars and so is expected to be strongly correlated with the underlying photometric-stellar mass of early-type galaxies. To illustrate this point, we computed the rest-frame  $H$ -band ( $\sim 1.6\mu\text{m}$ ) absolute magnitude,  $M_H$ , for our  $z \sim 1$  early-type galaxy sample, by applying an  $H$ -band filter transmission function to each best-fit model. In Figure 6, we plot  $M_H$  against the derived stellar mass resulting in a tight correlation. The dashed line corresponds to a straight-line fit to the data that yields:

$$\log \frac{M_{\text{phot}}}{M_{\odot}} = -((0.47 \pm 0.02) \cdot M_H + (0.3 \pm 0.1)) \quad (2)$$

## 5.2. Comparison with other stellar population synthesis models

As stated above, our photometric-stellar masses are derived by sampling the entire relevant wavelength domain of stellar light emission, from the rest-frame UV through the NIR. However, the reliability of spectrum synthesis models at  $\lambda_{\text{obs}} \sim 2\mu\text{m}$  has long been debated (Maraston (1998) and references therein).

In the rest-frame near-IR regime, in early stages of the galaxy evolution, a short-duration thermally pulsating (TP-) AGB phase is known to be relevant. The PEGASE.2 models we primarily use in our work compute isochrones up to the TP-AGB phase using the equations proposed by Groenewegen & de Jong (1993) (see also Fioc & Rocca-Volmerange (1996)).

Measuring the evolution of the rest-frame K-band FP from  $z \sim 1$  to the present, van der Wel et al. (2005) find the evolution in  $M/L_K$  to be slower than the evolution in  $M/L_B$ , as expected from stellar populations models. This study also finds the dust-free Maraston (2005) (M05) models (which implement the short-duration TP-AGB phases adopting a ‘fuel consumption’ approach) to provide a better fit to the data than dust-free Bruzual & Charlot (2003) (BC03) models (which implement the TP-AGB phases with an empirical prescription).

van der Wel et al. (2005) also suggest that the models uncertainties caused by the different treatment of AGB stars can severely hamper the determination of  $z \sim 1$  early-type galaxy

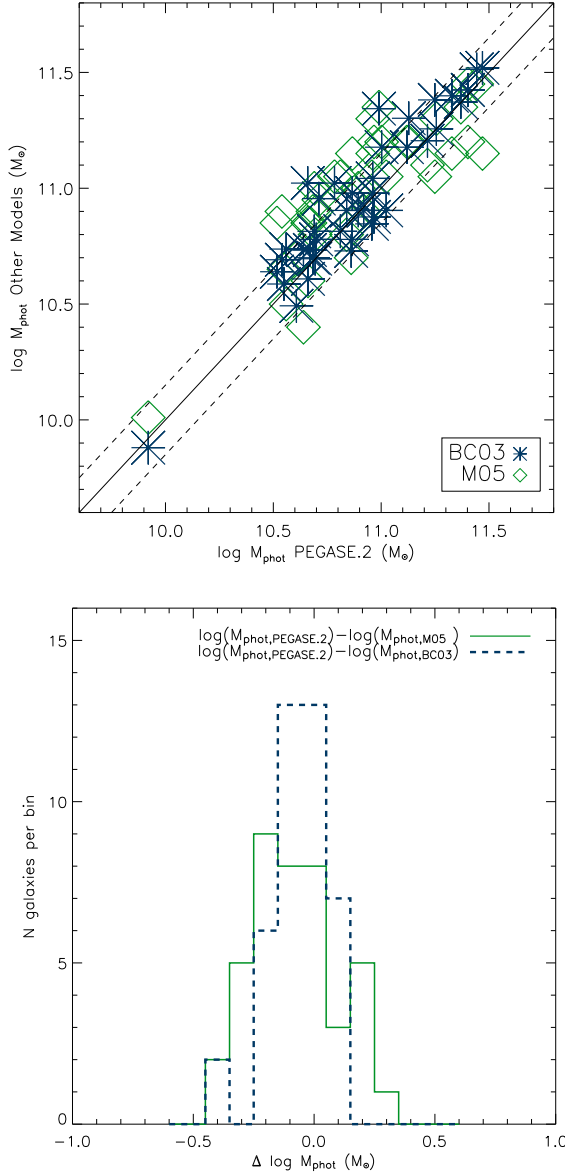


**Fig. 7.** Top panel: Comparison of different model predictions in determining photometric-stellar masses of early-type galaxies at  $z \sim 1$ . PEGASE.2 (Fioc & Rocca-Volmerange 1997) results are compared with Maraston (2005) and Bruzual & Charlot (2003) models, both with various exponentially-declining SFHs ( $0.1 < \tau < 10 \text{ Gyr}$ ), solar metallicity and Kroupa (2001) IMF (see text). The dashed lines indicate errors of 40%. Bottom panel: difference between PEGASE.2 and BC03 or M05 models mass estimates,  $\langle \Delta \log(M_{\text{phot}}/M_{\odot}) \rangle = -0.06, -0.08 \text{ dex}$ , and  $\sigma_{\Delta \log(M_{\text{phot}}/M_{\odot})} = 0.11, 0.17 \text{ dex}$ , respectively

masses from rest-frame near-IR photometry.

We compare our photometric-stellar mass estimates based on CSP dust-free PEGASE.2 models with those obtained with a set of dust-free CSPs models built with both Maraston (2005) and Bruzual & Charlot (2003) models, using exponentially-declining SFHs ( $0.1 < \tau < 10 \text{ Gyr}$ ), solar metallicity and

Kroupa (2001) IMF. Since M05 models provide calibrated spectra only up to  $2.5 \mu\text{m}$ , when using M05 models, we limit the SED fitting range to the  $4.5 \mu\text{m}$  IRAC channel. For our sample, we find consistent photometric-stellar mass estimates with CSPs PEGASE.2, M05 and BC03 models within typical errors of 40% (see top panel of Figure 7). The average difference between the photometric-stellar masses estimated with PEGASE.2 and BC03 or M05 model is  $\langle \Delta \log(M_{\text{phot}}/M_{\odot}) \rangle = -0.06 \text{ dex}$  and  $-0.08 \text{ dex}$  respectively, with a standard deviation of  $\sigma_{\Delta \log(M_{\text{phot}}/M_{\odot})} = 0.11 \text{ dex}$  and  $0.17 \text{ dex}$  (see bottom panel of Figure 7).

Thus, recognizing the uncertainties involved in the SED fitting technique and in the multiwavelength photometry, we find the overall difference in photometric-stellar mass estimates for early-type galaxies at  $z \sim 1$  from PEGASE.2, BC03, M05 not to be significant. This is not surprising. In fact, regardless of the actual implementation of the TP-AGB phase in the different codes, the rest-frame K-band is expected to be dominated by AGB stars only for  $0.1 < T_{\text{AGB}}/\text{Gyr} < 2.0$ , while we find our sample ages all to be much greater than 2 Gyr, in agreement with similar studies of  $z \sim 1.0$  early-type galaxies (Cimatti et al. (2002), Franx et al. (2003), Cimatti et al. (2004), Glazebrook et al. (2004), McCarthy et al. (2004), Fontana et al. (2004), Saracco et al. (2004), Rocca-Volmerange et al. (2004)). These results contrast with those of van der Wel et al. (2005), however a direct comparison is not possible since they adopted Simple Stellar Population models and different estimates of the photometric errors (weights) on the IRAC photometry.

## 6. Dynamical masses of early-type galaxies

The central velocity dispersion measures the random motions of the stars averaged along the line of sight through the galaxy, and is known to be a good tracer of the dynamical state of spheroidal, non rotationally-supported, galactic systems in virial equilibrium. The dynamical mass of a spherical, non-rotating, isotropic model with a Sérsic  $R^{1/n}$  SB profile is given by Bertin et al. (2002):

$$M_{\text{dyn}} = K_V(n, R_a) \frac{\sigma_a^2 R_{e,n}}{G}, \quad (3)$$

where  $\sigma_a$  is the velocity dispersion measured within an aperture of radius  $R_a$ , and  $K_V(n, R_a)$  is the so-called ‘virial coefficient’, that takes into account the differences between the virial and the effective radii, and between the virial and the observed velocity dispersions. If the galaxy SB profile is well described by the de Vaucouleurs law ( $n = 4$  in the previous equation) and if  $\sigma_a$  is the central velocity dispersion (measured within a tenth of the effective radius), the ‘classical’ value  $K_V \simeq 5$  (e.g., Michard (1980)) is recovered. Using high signal-to-noise (S/N) integral field spectroscopy of a sample of early-type galaxies at  $z \sim 0$  (the SAURON project; Bacon et al. (2001)), Cappellari et al. (2005) have recently found that the above expression with  $n = 4$  and  $K_V = 5.0 \pm 0.1$  reproduces the galaxy dynamical masses, closely matching the values obtained with

a much more accurate modelling (the so-called ‘Schwarzschild method’).

We use Eq. (3) with  $K_V$  properly computed taking into account our best-fitting values of  $n$  and  $R_{e,n}$  from the *HST*/ACS images, and the published, aperture-corrected velocity dispersions (following the prescriptions of Bertin et al. (2002) for apertures of radius  $R_J/R_{e,n}$ ). Note that the mass computed by such a relation corresponds to the galaxy *total* mass, and it is appropriate both for a single component (stars only), and for a two-component (stars and dark matter) system, provided that the dark matter density distribution parallels the stellar one (see Lanzoni & Ciotti (2003)). The values of each galaxy  $K_V$  and dynamical mass,  $M_{dyn}(K_V)$  are presented in Table 1.

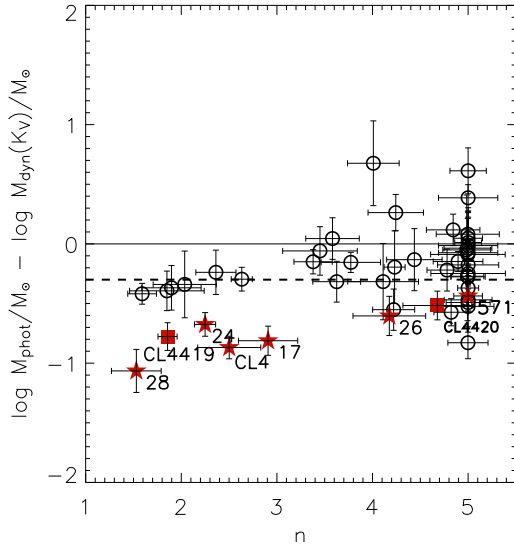


**Fig. 8.** Photometric-stellar vs dynamical mass differences,  $\log(M_{phot}) - \log(M_{dyn}(K_V))$ , as a function of the Sérsic index,  $n$ . Kroupa (2001) IMF is assumed. Adopting a Salpeter (1955) IMF all the  $\log M_{phot}$  values would constantly increase by  $\approx 0.3$  dex. This effect could be visualized by shifting the one-to-one line (the horizontal solid line) of 0.3 dex downward, to the position of the dashed line. Symbols are the same as in Fig. 4

## 7. Comparing photometric-stellar and dynamical mass estimates

Before discussing the direct comparison between photometric-stellar masses and total dynamical masses using Eq.(3), we describe some possible biases that may in principle affect both measurements.

As mentioned above, using the dynamical mass estimates rely on the simple assumption that an early-type galaxy is a spherical, isotropic, non rotationally-supported galactic system in virial equilibrium. The presence of a rotational component in the form of a disk or the presence of dynamical galaxy-to-galaxy interaction may have an effect which is not

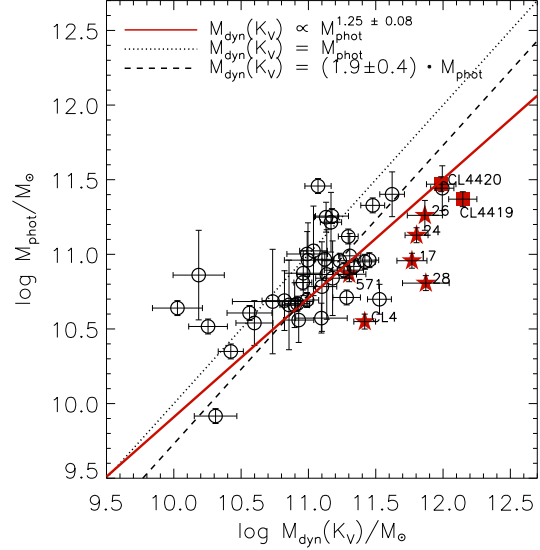


**Fig. 9.** Total dynamical,  $M_{dyn}(K_V)$ , vs. photometric-stellar,  $M_{phot}$ , mass estimates for the entire early-type galaxy sample at  $z \sim 1$ . Symbols are the same as in Figure 4. The dashed lines indicates the 1.5-sigma clipped mean offset of  $-0.27 \pm 0.09$  dex. The red dotted-dashed line show the best fit correlation between dynamical mass and photometric-stellar masses (see text).

easy to quantify.

In Figure 8, we plot mass differences for our sample,  $\log(M_{phot}) - \log(M_{dyn}(K_V))$ , against the Sérsic index,  $n$ . We generally find the mass deviation to be larger for  $n < 3$  galaxies.

The modulus of the differences of the bulgy-spiral sub-sample of Fig. 2 (indicated as filled red stars in Fig. 8) is larger than the average at any  $n$ ; with dynamical masses being larger than photometric-stellar masses with decreasing Sérsic indices. For these galaxies, the flattening of the SB profile reveals an increasing contribution of the disk component. As a result, their measured velocity dispersions, and thus the derived dynamical mass estimates, can be biased to larger values because of the presence of a rotating stellar disk which is generally included in the spectroscopic apertures ( $1''$ ) at these redshifts. This trend is also seen in recent observations by Ganda et al. (2005) of local spiral-galaxies using SAURON integral field spectroscopy. Their measured stellar kinematic maps often show a central depression in the velocity dispersion, with velocity dispersion profiles increasing outwards. However, one would also expect this effect to be maximum in case of edge-on galaxies and to be minimum/negligible for face-on galaxies. In our case, this would imply that at least for the face-on objects CDFS-24, CDFS-26, CDFS-571 and CL1252-4, the measured velocity dispersion is probably slightly affected by the presence of a disk.

Among the galaxies with dynamical masses significantly exceeding the photometric ones, we note in Fig. 8 the two



elliptical galaxies, CL4419 and CL4420 (filled red squares). These are the central Bright Cluster Galaxies (BCGs) of CL1252 which show signs of mutual dynamical interaction (see Fig. 3). Such interactions may, in principle, introduce anisotropies into the motion of their stars, thus affecting the  $\sigma_a$  measurements in a way that is not trivial. We also note that using field early-type galaxies and cluster BCGs in our study is justified by the results of van der Wel et al. (2005), who find that the most massive galaxies ( $M \gtrsim 10^{11} M_\odot$ ) lie on the same Fundamental Plane line regardless of their environments.

Photometric stellar mass estimates may also be affected by systematics. First, photometric-stellar masses weakly depend on the assumed model of dust extinction and metallicity evolution. Second and more importantly, they depend on the assumed IMF. For instance, by using a Salpeter (1955) IMF, instead of our adopted Kroupa (2001) IMF, all the  $\log M_{\text{phot}}$  values would be shifted upwards by  $\approx 0.3$  dex. In Fig. 8, this effect is shown by shifting the one-to-one line (the horizontal solid line) 0.3 dex downward, to the position of the dashed line. Adopting a Salpeter (1955) IMF a large number of galaxies would have photometric stellar masses greater than the dynamical ones, in agreement with the studies of Cappellari et al. (2005) and Ferreras et al. (2005) in local early-type galaxies, which also favour a Kroupa (2001) IMF. However, it is clear that our data cannot be used to constrain the choice of the IMF.

In Fig. 9, we present the direct comparison of total dynamical and photometric-stellar masses. We find that, adopting a Kroupa (2001) IMF, the photometric-stellar masses reproduce the dynamical ones with a 1.5-sigma clipped mean offset of  $-0.27 \pm 0.09$  dex (dashed line). This relation implies  $M_{\text{dyn}}(K_V) = (1.9 \pm 0.4) \cdot M_{\text{phot}}$  and it is illustrated in In Fig. 9. Therefore, if the IMF is not varying, this first result suggests the presence of a 40 – 50% dark matter component beyond several  $R_e$ .

We also compute (dotted-dashed red line) the best fit relation for the entire sample, which yields:

$$M_{\text{dyn}}(K_V) = 10^{(-2.4 \pm 0.9)} \cdot M_{\text{phot}}^{(1.25 \pm 0.08)}. \quad (4)$$

We note that the best-fit slope does not change if the bulge-dominated spirals (red stars) are excluded from the fit. We have also note that the relatively small error bar for the galaxy with  $\log M_{\text{phot}} < 10$ , does not have a significant impact on the determination of the best-fit slope either.

Our finding is in agreement with the picture of early-type galaxies, being dark matter dominated ( $M_{\text{dyn}} \gg M_{\text{phot}}$ ) in the most massive systems and baryon dominated ( $M_{\text{dyn}} \gtrsim M_{\text{phot}}$ ) in less massive systems, on scale of several  $R_e$ . The power law index in Eq. (4) is indeed consistent with completely independent estimates (at  $0.3 < z < 1.0$ ) of total mass using strong gravitational lensing by Ferreras et al. (2005). Accordingly, these authors find the dark matter dominating in massive elliptical galaxies while the stellar content dominates the mass budget in lower mass galaxies. In this context, the evolution of the dark matter fraction with the early-type galaxy mass has also been

commonly invoked as a possible explanation of the so-called ‘tilt’ of the FP (e.g., Ferreras & Silk (2000)).

## 8. Conclusions

In this work, we have used photometry from 9-10 passbands to build accurate SEDs, covering the 0.2-4  $\mu\text{m}$  rest-frame wavelengths, of a sample of 48 early-type galaxies at  $z \sim 1$  with published velocity dispersions. The large wavelength baseline and accuracy of our photometric measurements allows us to compare measured stellar masses with different spectrum synthesis models.

Based on our sample, which spans a limited mass range  $\log M_{\text{phot}} \simeq [10, 11.5]$ , corresponding to the bright end of the stellar mass function,  $M \gtrsim M^*$ , we find that photometric-stellar mass estimates are not strongly dependent on the choice of the stellar population model. Regardless of the actual implementation of the TP-AGB phase in the different codes, we find the overall difference in photometric-stellar masses of early-type galaxies at  $z \sim 1$  from PEGASE.2, BC03, M05 not to be statistically significant (below 0.1 dex).

We have also investigated the other inherent systematic uncertainties on stellar masses, such as those due to reddening and adopted IMF, and found them of the order 0.2-0.3 dex.

We have then compared our photometric-stellar masses to the total dynamical masses as inferred from velocity dispersion measurements and half-light radii measured in deep *HST*/ACS images. Strong deviations from  $M_{\text{dyn}} = M_{\text{phot}}$  may be ascribed to possible biases in dynamical mass measurements, as suggested by the evidence that deviations increase for early-type galaxies with small disk components and/or complex morphologies, as well as in galaxies showing signs of dynamical interaction with close-by companions. In the other hand, photometric-stellar masses depend on the assumed model of dust extinction and metallicity evolution as well as from the assumed IMF.

Assuming Kroupa (2001) IMF, we find the photometric-stellar masses to reproduce the dynamical mass estimates with an average offset of 0.27 dex. We note that the average offset depends on the assumed IMF, although a Salpeter (1955) IMF would produce unphysical results by implying that a large number of galaxies would have photometric-stellar masses greater than dynamical estimates.

We also find that an increasing dark matter fraction with the increasing total galaxy mass may be needed to explain the observed trend in  $M_{\text{dyn}}(K_V) \propto M_{\text{phot}}^{(1.25 \pm 0.08)}$ . It is reassuring that a similar relation and slope was found in studies where the galaxy mass was directly derived from strong lensing models. The increase in  $M_{\text{dyn}}/M_{\text{phot}}$  with increasing dynamical mass that we find is consistent with the increase of the mass-to-light ratio ( $M_{\text{dyn}}/L$ ) of early type galaxies implied by FP studies.

We conclude that the determination of photometric stellar masses of massive early-type galaxies at  $z \sim 1$  is robust against stellar population models, when a large wavelength baseline is available, and its accuracy hinges primarily on the adopted IMF.

Although a clear correlation  $M_{\text{dyn}} - M_{\text{phot}}$  is found, it remains

difficult to use photometric masses as reliable surrogates of total galaxy masses, or mass-to-light ratios, over a wide mass range. Specifically, it would be interesting to extend our study to less massive galaxies ( $M_{\text{phot}} < 10^{10} M_{\odot}$ ) with possibly younger ages, not probed by our sample. Further studies on galaxy-scale lensing systems (e.g., (Koopmans & Treu 2003)), with masses accurately determined by parameter free strong lensing models, will surely stimulate significant progress in the years to come.

*Acknowledgements.* A.R. is very grateful to A. Renzini, G. Zamorani, J. Vernet and M. Pannella for useful discussions.

RAEF is affiliated to the Research and Science Support Department of the European Space Agency. The work of DS was carried out at Jet Propulsion Laboratory, California Institute of Technology, under a contract with NASA. The work by SAS was performed under the auspices of the U.S. Department of Energy, National Nuclear Security Administration by the University of California, Lawrence Livermore National Laboratory under contract No. W-7405-Eng-48.

## References

- Bacon, R., Copin, Y., Monnet, G., et al. 2001, *MNRAS*, 326, 23
- Baugh, C. M., Benson, A. J., Cole, S., Frenk, C. S., & Lacey, C. 2003, in *The Mass of Galaxies at Low and High Redshift*, 91–+
- Bertin, G., Ciotti, L., & Del Principe, M. 2002, *A&A*, 386, 149
- Blakeslee, J. P., Franx, M., Postman, M., et al. 2003, *ApJ*, 596, L143
- Bohlin, R. C., Cornett, R. H., Hill, J. K., et al. 1991, *ApJ*, 368, 12
- Brinchmann, J. & Ellis, R. S. 2000, *ApJ*, 536, L77
- Bruzual, G. & Charlot, S. 2003, *MNRAS*, 344, 1000
- Busarello, G., Capaccioli, M., Capozziello, S., Longo, G., & Puddu, E. 1997, *A&A*, 320, 415
- Caon, N., Capaccioli, M., & D’Onofrio, M. 1993, *MNRAS*, 265, 1013
- Capaccioli, M. 1989, in *World of Galaxies (Le Monde des Galaxies)*, 208–227
- Cappellari, M., Bacon, R., Bureau, M., et al. 2005, *astro-ph/0505042*
- Cardelli, J. A., Clayton, G. C., & Mathis, J. S. 1989, *ApJ*, 345, 245
- Cimatti, A., Daddi, E., Renzini, A., et al. 2004, *Nature*, 430, 184
- Cimatti, A., Pozzetti, L., Mignoli, M., et al. 2002, *A&A*, 391, L1
- Cohen, J. G., Hogg, D. W., Pahre, M. A., et al. 1999, *ApJS*, 120, 171
- Cole, S., Norberg, P., Baugh, C. M., et al. 2001, *MNRAS*, 326, 255
- De Lucia, G., Springel, V., White, S. D. M., Croton, D., & Kauffmann, G. 2005, *astro-ph/0509725*
- di Serego Alighieri, S., Vernet, J., Cimatti, A., et al. 2005, *A&A*, 442, 125
- Dickinson, M., Papovich, C., Ferguson, H. C., & Budavári, T. 2003, *ApJ*, 587, 25
- Djorgovski, S. & Davis, M. 1987, *ApJ*, 313, 59
- D’Onofrio, M., Capaccioli, M., & Caon, N. 1994, *MNRAS*, 271, 523
- Dressler, A. 1987, *ApJ*, 317, 1
- Drory, N., Bender, R., Feulner, G., et al. 2004a, *ApJ*, 608, 742
- Drory, N., Bender, R., & Hopp, U. 2004b, *ApJ*, 616, L103
- Drory, N., Bender, R., Snigula, J., et al. 2001, *ApJ*, 562, L111
- Fazio, G. G., Hora, J. L., Allen, L. E., et al. 2004, *ApJS*, 154, 10
- Ferreras, I., Saha, P., & Williams, L. L. R. 2005, *ApJ*, 623, L5
- Ferreras, I. & Silk, J. 2000, *MNRAS*, 316, 786
- Fioc, M. & Rocca-Volmerange, B. 1996, in *ASP Conf. Ser.* 98, 67–+
- Fioc, M. & Rocca-Volmerange, B. 1997, *A&A*, 326, 950
- Fioc, M. & Rocca-Volmerange, B. 1999, *A&A*, 344, 393
- Fontana, A., Donnarumma, I., Vanzella, E., et al. 2003, *ApJ*, 594, L9
- Fontana, A., Pozzetti, L., Donnarumma, I., et al. 2004, *A&A*, 424, 23
- Franx, M. 1993, *PASP*, 105, 1058
- Franx, M., Labbé, I., Rudnick, G., et al. 2003, *ApJ*, 587, L79
- Ganda, K., Falcon-Barroso, J., Peletier, R., et al. 2005, *astro-ph/0512304*
- Gavazzi, G., Pierini, D., & Boselli, A. 1996, *A&A*, 312, 397
- Gebhardt, K., Faber, S. M., Koo, D. C., et al. 2003, *ApJ*, 597, 239
- Gerhard, O., Kronawitter, A., Saglia, R. P., & Bender, R. 2001, *AJ*, 121, 1936
- Gialalisco, M., Ferguson, H. C., Koekemoer, A. M., et al. 2004, *ApJ*, 600, L93
- Gialalisco, M., Livio, M., Bohlin, R. C., Macchetto, F. D., & Stecher, T. P. 1996, *AJ*, 112, 369
- Glazebrook, K., Abraham, R. G., McCarthy, P. J., et al. 2004, *Nature*, 430, 181
- Graham, A., Lauer, T. R., Colless, M., & Postman, M. 1996, *ApJ*, 465, 534
- Groenewegen, M. A. T. & de Jong, T. 1993, *A&A*, 267, 410
- Hernquist, L. & Springel, V. 2003, *MNRAS*, 341, 1253
- Holden, B. P., van der Wel, A., Franx, M., et al. 2005, *ApJ*, 620, L83
- Jorgensen, I., Franx, M., & Kjaergaard, P. 1995, *MNRAS*, 276, 1341
- Kauffmann, G., Heckman, T. M., White, S. D. M., et al. 2003, *MNRAS*, 341, 54
- Koopmans, L. V. E. & Treu, T. 2003, *ApJ*, 583, 606
- Kroupa, P. 2001, *MNRAS*, 322, 231
- Kuchinski, L. E., Freedman, W. L., Madore, B. F., et al. 2000, *ApJS*, 131, 441
- Lanzoni, B. & Ciotti, L. 2003, *A&A*, 404, 819
- Le Borgne, D. & Rocca-Volmerange, B. 2002, *A&A*, 386, 446
- Lidman, C., Rosati, P., Demarco, R., et al. 2004, *A&A*, 416, 829
- Lintott, C., Ferreras, I., & Lahav, O. 2005, *ArXiv Astrophysics e-prints*
- Maraston, C. 1998, *MNRAS*, 300, 872
- Maraston, C. 2005, *MNRAS*, 362, 799
- Marleau, F. R. & Simard, L. 1998, *ApJ*, 507, 585
- McCarthy, P. J., Le Borgne, D., Crampton, D., et al. 2004, *ApJ*, 614, L9

- Michard, R. 1980, *A&A*, 91, 122
- Nagamine, K., Cen, R., Hernquist, L., Ostriker, J. P., & Springel, V. 2004, *ApJ*, 610, 45
- Napolitano, N. R., Capaccioli, M., Romanowsky, A. J., et al. 2005, *MNRAS*, 357, 691
- Papovich, C., Dickinson, M., & Ferguson, H. C. 2001, *ApJ*, 559, 620
- Papovich, C., Giavalisco, M., Dickinson, M., Conselice, C. J., & Ferguson, H. C. 2003, *ApJ*, 598, 827
- Ravindranath, S., Giavalisco, M., Ferguson, H. C., et al. 2006, *ArXiv Astrophysics e-prints*
- Rocca-Volmerange, B., Le Borgne, D., & De Breuck, C. e. a. 2004, *A&A*, 415, 931
- Rosati, P., Tozzi, P., Ettori, S., et al. 2004, *AJ*, 127, 230
- Rudnick, G., Rix, H.-W., Franx, M., et al. 2003, *ApJ*, 599, 847
- Rusin, D. & Kochanek, C. S. 2005, *ApJ*, 623, 666
- Salpeter, E. E. 1955, *ApJ*, 121, 161
- Saracco, P., Longhetti, M., Giallongo, E., et al. 2004, *A&A*, 420, 125
- Sersic, J. L. 1968, *Atlas de galaxias australes* (Cordoba, Argentina: Obs. Astronomico, 1968)
- Shapley, A. E., Steidel, C. C., Adelberger, K. L., et al. 2001, *ApJ*, 562, 95
- Simard, L. 1998, in *ASP Conf. Ser.* 145, 108–+
- Somerville, R. S., Moustakas, L. A., Mobasher, B., et al. 2004, *ApJ*, 600, L135
- Songaila, A., Cowie, L. L., Hu, E. M., & Gardner, J. P. 1994, *ApJS*, 94, 461
- Spergel, D. N., Verde, L., Peiris, H. V., et al. 2003, *ApJS*, 148, 175
- Thomas, J., Saglia, R. P., Bender, R., et al. 2005, *MNRAS*, 360, 1355
- Treu, T., Ellis, R. S., Liao, T. X., et al. 2005, *ApJ*, 633, 174
- Treu, T. & Koopmans, L. V. E. 2004, *ApJ*, 611, 739
- Treu, T., Stiavelli, M., Bertin, G., Casertano, S., & Møller, P. 2001, *MNRAS*, 326, 237
- van der Wel, A., Franx, M., van Dokkum, P. G., et al. 2005, *astro-ph/0511581*
- van der Wel, A., Franx, M., van Dokkum, P. G., et al. 2005, *ApJ*, 631, 145
- van Dokkum, P. G. & Franx, M. 1996, *MNRAS*, 281, 985
- van Dokkum, P. G., Franx, M., Kelson, D. D., & Illingworth, G. D. 1998, *ApJ*, 504, L17+
- Vazdekis, A. 1999, *ApJ*, 513, 224
- Vazdekis, A., Casuso, E., Peletier, R. F., & Beckman, J. E. 1996, *ApJS*, 106, 307
- York, D. G., Adelman, J., Anderson, J. E., et al. 2000, *AJ*, 120, 1579

**Table 1.** The early-type galaxy sample at  $z \sim 1$ . IDs are from the original surveys and the reader is referred to the aforementioned papers for objects selection and coordinates.  $z_{F850lp}$  is the  $3''$  aperture magnitude in the *HST*/ACS *F850lp* filter;  $M_H$  is the rest-frame absolute magnitude obtained applying an *H*-band standard filter transmission function to each best-fit model;  $U - V$  is a rest-frame color. The magnitudes and the color are in the AB system. Only statistical errors are quoted for photometric-stellar masses.

ID	$z_{spec}$	$z_{F850lp}$ (mag)	$M_H$ (mag)	$U - V$	$n$	$R_{e,n}$ (kpc)	$K_V$	$\sigma_0$ (km/s)	$\log \frac{M_{dyn}(K_V)}{M_\odot}$	$\log \frac{M_{phot}}{M_\odot}$
CDFS-1	1.089	21.18	-24.05	1.68	3.63±0.25	3.17±0.12	5.15±0.21	231± 15	11.31±0.08	10.99±0.15
CDFS-2	0.964	20.75	-23.91	1.80	5.00±0.32	5.45±0.21	3.90±0.22	200±9	11.30±0.07	11.12±0.05
CDFS-3	1.044	21.78	-23.33	1.73	4.11±0.37	1.07±0.05	5.61±0.24	300± 30	11.10±0.11	10.78±0.30
CDFS-4	0.964	20.66	-24.66	1.99	4.22±0.22	8.42±0.53	4.47±0.22	336± 18	11.99±0.09	11.44±0.15
CDFS-5	0.685	21.31	-22.80	1.99	2.63±0.11	1.79±0.09	6.24±0.09	194± 15	10.99±0.09	10.69±0.05
CDFS-6	0.660	20.58	-22.79	1.81	5.00±0.39	1.81±0.18	4.55±0.23	208±9	10.92±0.09	10.67±0.05
CDFS-7	1.135	21.43	-24.53	1.93	5.00±0.33	3.18±0.34	3.76±0.21	232± 19	11.18±0.12	11.26±0.05
CDFS-8	1.125	22.21	-23.18	1.87	4.99±0.17	2.07±0.18	4.45±0.10	253± 70	11.14±0.22	10.86±0.30
CDFS-9	1.097	21.78	-23.92	1.65	5.00±0.25	2.08±0.10	4.44±0.14	215± 45	11.00±0.18	10.96±0.25
CDFS-10	1.119	22.08	-23.30	1.68	4.44±0.29	0.62±0.05	6.06±0.19	275± 49	10.82±0.17	10.69±0.20
CDFS-11	1.096	22.07	-23.77	1.96	5.00±0.14	2.39±0.18	4.07±0.09	208± 33	10.99±0.15	11.00±0.15
CDFS-12	1.123	21.80	-23.69	1.85	5.00±0.31	1.44±0.11	4.76±0.18	262± 20	11.04±0.10	11.02±0.30
CDFS-13	0.980	20.76	-24.05	1.87	5.00±0.15	2.58±0.24	4.02±0.10	247± 10	11.17±0.08	11.21±0.20
CDFS-14	0.984	21.59	-23.71	1.65	5.00±0.18	4.80±0.54	3.95±0.12	197± 21	11.23±0.13	10.96±0.05
CDFS-15	0.622	20.77	-22.92	1.98	5.00±0.21	3.53±0.22	4.09±0.13	317± 21	11.53±0.09	10.70±0.10
CDFS-16	0.669	20.70	-23.30	1.99	5.00±0.11	2.85±0.31	4.03±0.06	262± 36	11.26±0.15	10.89±0.05
CDFS-17	0.954	21.39	-23.71	1.64	2.91±0.31	4.65±0.13	5.84±0.36	305± 31	11.77±0.11	10.96±0.05
CDFS-20	1.022	21.26	-24.29	1.98	4.84±0.28	3.50±0.08	4.20±0.19	199± 15	11.13±0.09	11.25±0.10
CDFS-21	0.735	21.07	-22.51	1.63	5.00±0.31	1.05±0.10	4.90±0.18	149±8	10.42±0.09	10.35±0.05
CDFS-22	0.735	20.68	-23.63	1.71	5.00±0.25	5.88±0.31	3.79±0.17	225± 11	11.42±0.08	10.95±0.05
CDFS-23	1.041	22.04	-23.05	1.90	4.01±0.27	2.74±0.22	4.91±0.20	70± 15	10.18±0.19	10.86±0.30
CDFS-24	1.042	21.10	-24.06	1.79	2.25±0.11	9.13±0.35	6.79±0.18	210± 16	11.80±0.09	11.13±0.05
CDFS-25	0.967	21.55	-23.32	1.85	5.00±0.39	1.20±0.23	4.95±0.23	258± 18	10.96±0.14	10.87±0.15
CDFS-26	1.129	21.24	-24.67	1.65	4.18±0.38	11.17±0.64	4.55±0.42	249± 25	11.86±0.13	11.26±0.10
CDFS-27	1.128	21.95	-23.37	1.42	5.00±0.27	7.84±0.45	3.76±0.20	135± 30	11.10±0.19	10.57±0.10
CDFS-28	0.954	21.85	-23.34	1.65	1.53±0.26	2.29±0.21	7.08±0.15	445± 84	11.87±0.17	10.81±0.05
CDFS-29	1.128	21.07	-24.42	1.92	5.00±0.31	2.39±0.13	4.34±0.19	221± 17	11.07±0.10	11.46±0.05
CL1252-1	0.671	20.61	-23.29	1.65	4.82±0.18	4.27±0.54	4.04±0.12	219± 12	11.28±0.10	10.71±0.05
CL1252-2	0.658	20.88	-22.55	1.90	4.23±0.11	1.23±0.07	5.39±0.07	216±6	10.86±0.05	10.66±0.30
CL1252-3	0.844	20.46	-24.08	1.49	1.59±0.15	4.75±0.37	7.14±0.12	166±7	11.34±0.07	10.92±0.05
CL1252-4	0.743	20.61	-23.01	1.63	2.50±0.33	4.37±0.27	6.31±0.40	202±8	11.42±0.08	10.55±0.05
CL1252-5	0.743	20.35	-23.92	1.65	5.00±0.23	4.91±0.31	3.94±0.15	251±9	11.45±0.07	10.96±0.05
CL1252-6	0.734	20.68	-23.54	1.65	4.89±0.26	1.92±0.16	4.57±0.16	211±5	10.96±0.07	10.81±0.05
CL1252-7	0.753	20.16	-24.04	1.57	3.77±0.31	2.43±0.19	5.16±0.23	213±5	11.12±0.07	10.97±0.05
CL1252-8	1.069	21.98	-23.17	1.68	5.00±0.19	2.71±0.25	4.25±0.12	63± 13	10.03±0.19	10.64±0.05
CL1252-9	1.036	22.20	-22.92	1.57	4.24±0.29	1.42±0.06	5.24±0.19	102± 16	10.25±0.14	10.52±0.05
CDFS-369	0.894	22.31	-21.64	1.35	1.85±0.39	0.84±0.05	7.36±0.20	119± 21	10.31±0.16	9.92±0.05
CDFS-467	0.895	21.54	-22.92	1.68	3.45±0.39	1.52±0.10	5.72±0.28	140± 18	10.60±0.14	10.54±0.15
CDFS-532	1.215	22.13	-23.67	1.68	2.04±0.33	1.41±0.10	6.82±0.23	260± 30	11.18±0.13	10.84±0.25
CDFS-547	1.222	22.03	-23.19	1.50	1.90±0.31	0.74±0.04	7.50±0.16	256± 28	10.93±0.11	10.56±0.15
CDFS-571	0.955	21.22	-23.79	1.57	5.00±0.15	6.81±0.48	3.83±0.11	182± 21	11.30±0.12	10.87±0.05
CDFS-590	1.222	22.71	-23.08	1.73	4.99±0.25	4.09±0.52	4.03±0.16	119± 49	10.73±0.30	10.68±0.35
CDFS-633	1.096	21.04	-24.77	1.96	4.78±0.21	6.66±0.12	4.00±0.16	260± 23	11.62±0.09	11.40±0.15
CDFS-354	0.667	21.09	-22.84	1.65	3.58±0.28	3.08±0.12	5.20±0.24	99± 19	10.56±0.17	10.61±0.05
CL1252-6106	1.235	21.40	-24.56	1.79	3.38±0.20	2.76±0.35	5.42±0.17	294± 10	11.48±0.09	11.33±0.05
CL1252-9077	1.241	22.06	-23.44	1.50	2.36±0.21	3.15±0.11	6.38±0.23	130± 14	10.90±0.11	10.66±0.15
CL1252-4419	1.238	21.32	-24.54	1.81	1.86±0.10	8.56±0.84	7.72±0.12	302± 24	12.15±0.10	11.37±0.05
CL1252-4420	1.234	21.37	-24.68	1.86	4.68±0.36	9.82±0.77	4.07±0.32	323± 21	11.99±0.11	11.47±0.05